Facile synthesis of mono-disperse sub-20 nm $NaY(WO_4)_2:Er^{3+},Yb^{3+}$ upconversion nanoparticles: a new choice for nanothermometry†

Mei Lin,[a] Liujing Xie,[a] Zijun Wang,[ab] Bryce S. Richards,[cd] Guojun Gao *[c] and Jiuping Zhong *[a]

We report a novel optical nanothermometer based on ultra-small $NaY(WO_4)_2:Er^{3+},Yb^{3+}$ (NYW:Yb,Er) upconversion nanoparticles (UCNPs). The monodisperse, diamond-shaped sub-20 nm NYW:Er,Yb UCNPs with an average size of ~8.5 × 12.5 nm were prepared *via* a facile one-step thermolysis protocol. Upon 980 nm laser excitation, the NYW:Er,Yb UCNPs yield bright green UC emission. The maximum relative sensitivity (S_{rel}) and absolute sensitivity (S_{abs}) were determined to be ~1.2% K ^{1} at 293 K and ~0.9% K ^{1} at 503 K, respectively. The excellent repeatability of fluorescence intensity ratio (FIR) and low temperature uncertainty ΔT_{min} of ~0.4 K at 293 K make them promising for optical nanothermometry covering a wide temperature range of 293 503 K.

1. Introduction

Upconversion (UC) is an anti-Stokes process of converting two or more low energy photons to one high energy photon. In the last decade, rare-earth activated UC nanoparticles (UCNPs) have been rapidly developed due to their broad applicability in many fields, such as bio-imaging, drug delivery and optical thermometry.[1–5] Recently, UCNPs have been reported as one of the best candidates for nanothermometry.[6–10] Optical nanothermometry based on UCNPs can provide a contactless and non-invasive approach to map the temperature of the environment and human body.[11–13] The non-contact optical thermometer technology strongly relies on the variation of fluorescence intensity ratio (FIR) of two emission lines arising from two thermally coupled levels of trivalent rare earth ions.[10] Er^{3+} is the most popular activator based on its green UC emission originating from the two thermally coupled levels (TCLs) of $^2H_{11/2}$ and $^4S_{3/2}$. The energy gap ΔE between them is 700–800 cm^{-1}, which matches the requirement of 200 $cm^{-1} < \Delta E < 2000$ cm^{-1} well for effective thermal coupling in optical thermometry.[14,15]

To date, Yb^{3+}/Er^{3+} activated UC materials including fluorides, oxides, oxyfluorides and oxysulfides have been frequently reported as excellent candidates for optical thermometry.[11,13,16–19] Among them, β-$NaYF_4$:Yb,Er UCNPs have been recognized as promising candidates for nanothermometry due to their well-controlled morphology, small particle size of <50 nm, narrow size distribution and high UC emission efficiency due to their low phonon energy. Compared with fluorides, oxide materials present the advantages of easy preparation, good thermal conductivity, isotropic optical properties, and excellent thermal, mechanical and chemical stability.[9,20,21] Consequently, rare earth activated oxide phosphors have been found wide applications in many fields.[22] However, rare earth activated oxide nanoparticles typically exhibit properties of poor morphology control, large particle size (>50 nm), and broad size distribution, which strongly limit their application in the field of optical nanothermometry.[23–28]

Herein, we successfully synthesized monodisperse, diamond-shaped sub-20 nm $NaY(WO_4)_2:Er^{3+},Yb^{3+}$ (NYW:Yb,Er) UCNPs *via* a facile one-step thermolysis protocol.[29] Under excitation of 980 nm continuous laser, the NYW:Er,Yb UCNPs present a bright green color output to the naked eye. Based on the FIR technique, we monitored the samples in the temperature range of 293–503 K. The maximum relative sensitivity (S_{rel}) was determined to be ~1.2% K^{-1} at 293 K (physiological temperature region) and it decreases from ~1.2% K^{-1} at 293 K to ~0.4% K^{-1} at 503 K. It was found that the absolute sensitivity (S_{abs}) increased with temperature from ~0.6% K^{-1} at 293 K to the maximum ~0.9% K^{-1} at 503 K. A low temperature uncertainty of 0.4 K (293 K) based on the S_{rel} value was confirmed. The FIR of NYW:Er,Yb UCNPs shows excellent repeatability over two heating and cooling cycles

[a] School of Chemistry, School of Materials, Sun Yat sen University, Guangzhou 510275, China. E mail: Zhongjp@mail.sysu.edu.cn
[b] Condensed Matter and Interfaces, Debye Institute for Nanomaterials Science, Utrecht University, Princetonplein 1, 3584 CC Utrecht, The Netherlands
[c] Institute of Microstructure Technology, Karlsruhe Institute of Technology, 76344 Eggenstein Leopoldshafen, Germany. E mail: guojun.gao@kit.edu
[d] Light Technology Institute, Karlsruhe Institute of Technology, Engesserstrasse 13, 76131 Karlsruhe, Germany

over 293–503 K. These results suggest that NYW:Er^{3+},Yb^{3+} UCNPs are promising candidates for nanothermometry.

2. Experimental

2.1 Materials

High purity absolute ethanol (A.R.), cyclohexane (A.R.), oleic acid (A.R.), oleylamine (80–90%), 1-octadecene (>90%), yttrium(III) acetate tetrahydrate (99.9%), erbium(III) acetate hydrate (99.9%), ytterbium(III) acetate hydrate (99.9%), hexacarbonyl tungsten (97%), and sodium hydroxide (A.R.) were used as raw materials without further purification.

2.2 Synthesis of the $NaY_{(100-x-y)/100}(WO_4)_2$:*x*Er,*y*Yb nanoparticles

Double tungstate nanocrystals with nominal compositions of $NaY_{(99.5-x)/100}Yb_{x/100}Er_{0.005}(WO_4)_2$ (NYW:*x*Yb,0.5Er, x = 5, 10, 15, 20, and 25) and $NaY_{(80-y)/100}Yb_{0.2}Er_{y/100}(WO_4)_2$ (NYW:20Yb,*y*Er, y = 0.1, 0.2, 0.5, 1, 1.2 and 1.5) were synthesized *via* a one-step thermolysis protocol *via* the modification of the synthetic procedures for fluorides described in the literature.[29,30] In a typical procedure, oleic acid (10 mL), oleylamine (10 mL) and 1-octadecene (20 mL) were mixed in a 150 mL three-necked flask and heated at 150 °C for 1 h under vacuum to remove dissolved water. When the solution had been cooled to room temperature, the rare-earth ion(III) acetate (1 mmol), hexacarbonyl tungsten (2 mmol) and sodium hydroxide (1.5 mmol) were added to the cooled solution. The obtained solution was stirred at room temperature for 30 mins and then heated at 300 °C for 2 h under a protective nitrogen atmosphere. The nanoparticles were precipitated by addition of ethanol, collected by centrifugation (10 000 rpm, 5 min), washed several times with ethanol and dispersed in hexane, and then dried at 80 °C overnight. The final nanocrystals can be re-dispersed in nonpolar solvents, such as cyclohexane.

2.3 Characterization

The X-ray diffraction (XRD) patterns were recorded using a D-MAX 2200 VPC (Japan) X-ray diffractometer (Cu Kα radiation, λ = 1.5406 Å) with 2θ ranging from 10° to 70°, a step of 0.02° and an integration time of 1 s. Transmission electronic microscopy (TEM), high-resolution TEM (HRTEM) and selected area electron diffraction (SAED) were performed on an FEI Tecnai G2 F30 operating at 300 kV. A statistical center distance distribution histogram was estimated by software (J-image) based on the obtained digital TEM images. The UC emission spectra, luminescence decay curves at room temperature and temperature dependent UC emission spectra were measured on an Edinburgh Instruments FLS 980 spectrometer. A power tunable 980 nm continuous-wave diode laser was used as the excitation source and a photomultiplier tube (Hamamatsu R928P) was used as the detector. For temperature dependent UC emission measurements, the samples were loaded in a small custom-made chamber (Oxford Optistat DN liquid nitrogen cryostat) and the temperature was controlled with an accuracy of ±0.1 K (Oxford variable temperature device) *via* a thermocouple located next to the sample.

3. Results and discussion

3.1 Structure and morphology

Fig. 1a shows the X-ray diffraction (XRD) patterns of the NYW:*x*Yb,0.5Er (x = 5, 10, 15, 20 and 25) UC nanoparticles (UCNPs) as a function of Er^{3+} concentration. The diffraction

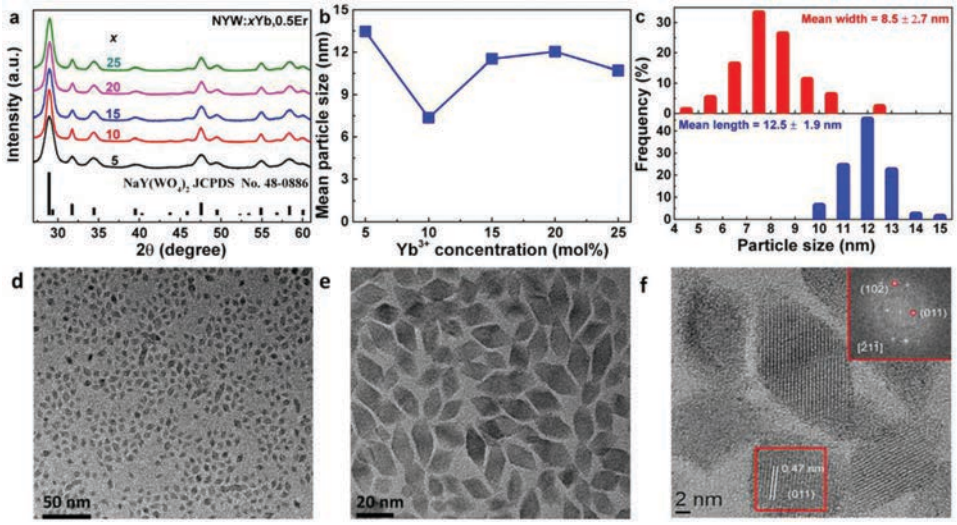

Fig. 1 (a) XRD patterns of NYW:20Yb,*y*Er (y = 0.1, 0.2, 0.5, 1, 1.2 and 1.5) UCNPs as a function of Er^{3+} concentration, with the standard XRD pattern of $NaY(WO_4)_2$ JCPDS card no. 48 0886 provided as a reference. (b) The dependence of the average particle size (calculated using eqn (1)) on Er^{3+} concentration. (c) Statistical center distance distribution histogram in two directions for NYW:20Yb,0.5Er UCNPs estimated using J image software based on TEM images. (d and e) TEM images of the NYW:20Yb,0.5Er UCNPs with different magnification. (f) HRTEM image of NYW:20Yb,0.5Er UCNPs and inset is the corresponding SAED pattern.

patterns of the NYW:*x*Yb,0.5Er UCNPs coincide well with the standard JCPDS card of $NaY(WO_4)_2$ [JCPDS: no. 48-0886; space group: $I41/a$ S (88)] following the well-known scheelite crystal structure of tetragonal $CaWO_4$.[31] The single crystal phase nature suggests that Yb^{3+} and Er^{3+} have been incorporated into the NYW crystal phase. This is ascribed to the similar ionic radii and same valence state of Y^{3+} (0.90 Å, eight-fold coordination) and Yb^{3+}/Er^{3+} (0.86/0.88 Å, eight-fold coordination).[32] Interestingly, the full width at half maximum (FWHM) of all diffraction peaks of NYW:*x*Yb,0.5Er is much wider than that of the micro-sized counterpart, which is a clear sign of the formation of nanoparticles. Based on the well-known Debye–Scherrer formula, the average size of nanoparticles can be estimated *via* eqn (1):[33]

$$D = K/(B\cos\theta) \quad (1)$$

where λ is the X-ray wavelength (λ = 1.5406 Å); θ is the Bragg angle of the diffraction peak, K is the Scherrer constant, which is set to 1.0; and B is the FWHM of the given diffraction peak. In the present case, the strongest diffraction peak at 2θ degree of $\sim$28.9° was chosen for evaluation *via* eqn (1). The average size was calculated to be $\sim$12 nm for the NYW:*x*Yb,0.5Er UCNPs (see Fig. 1b). XRD patterns of the NYW:20Yb,*y*Er (y = 0.1, 0.2, 0.5, 1, 1.2 and 1.5) UCNPs as a function of Er^{3+} doping concentration present similar behavior to those of NYW:*x*Yb,0.5Er (see Fig. S1, ESI†).

TEM was used to investigate the morphology and particle size distribution of the obtained UCNPs, as shown in Fig. 1c–f. The morphology of NYW is monodisperse diamond-shaped nanoparticles.[29] As shown in Fig. 1c, the statistical average width × length of the NYW:20Yb,0.5Er UCNPs was estimated to be (8.5 ± 2.7) nm × (12.5 ± 1.9) nm, which is close to that calculated by the Debye–Scherrer equation, as shown in Fig. 1b. It is noteworthy that the particle size is smaller and the size distribution is more homogeneous than typical oxide-based nanomaterials.[23–26] The HRTEM image presented an interplanar spacing of 3.1 and 4.7 Å, which correspond to the d spacings of the (112) and (101) planes of tetragonal $NaY(WO_4)_2$, respectively. The corresponding SAED pattern (see inset of Fig. 1f) reveals a pattern of tetragonal $NaY(WO_4)_2$, which well-matches the XRD result in Fig. 1a. On the basis of these results and the symmetry of the crystal lattice of tetragonal $NaY(WO_4)_2$, it can be concluded that the NYW nanocrystals are enclosed by (011) and (101) facets.

3.2 UC luminescence properties

The UC emission spectra of NYW:*x*Yb,0.5Er and the NYW:20Yb,*y*Er UCNPs as a function of Er^{3+} and Yb^{3+} concentration upon excitation of a 980 nm laser with a power density (PD) of 4 W cm^{-2} are plotted in Fig. 2a and c, respectively. The UC emission spectra of NYW:Yb,Er are composed of two distinct parts in green and red. The red UC band ranging from 640 to 680 nm with a maximum at 656 nm is attributed to the infra-configuration 4f → 4f electronic transition of Er^{3+}:$^4F_{9/2}$ → $^4I_{15/2}$. The green band ranging from 510 to 570 nm comprises two bands with maxima at 530 and 552 nm, which are attributed to the infra-configuration 4f → 4f electronic transitions of Er^{3+}: $^2H_{11/2}$ → $^4I_{15/2}$ and Er^{3+}: $^4S_{3/2}$ → $^4I_{15/2}$, respectively.[20] The emission intensity of the green band is $\sim$2 times stronger than that of the red band at room temperature leading to a pure green output color due to the poor sensitivity of the human eye in the deep red spectral region. This is demonstrated by the inset in Fig. 2a, which shows the emission photograph upon irradiation of a 980 nm laser (4 W cm^{-2}) in a dark environment. As mentioned in the introduction, the energy gap between $^2H_{11/2}$ and $^4S_{3/2}$ levels is $\sim$700–800 cm^{-1}. They are typical TCLs and very suitable for fluorescent ratiometric thermometers, which will be discussed later. The emission from the $^2H_{11/2}$ and $^4S_{3/2}$ levels is defined as G_1 and G_2, respectively.

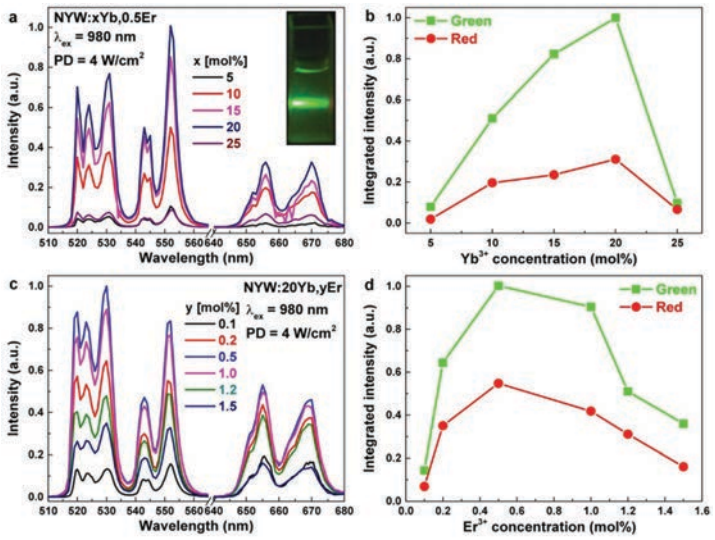

Fig. 2 The UC emission spectra of NYW:*x*Yb,0.5Er (x = 5, 10, 15, 20 and 25) and NYW:20Yb,*y*Er (y = 0.1, 0.2, 0.5, 1.0, 1.2 and 1.5) UCNPs as a function of Yb^{3+} (a) and Er^{3+} (c) concentration, respectively. The excitation source is a 980 nm laser (PD = 4 W cm^{-2}). Inset in (a): photograph of the NYW:20Yb,0.5Er UCNPs dispersed in cyclohexane solutions under excitation of an 8 W cm^{-2} 980 nm laser. The dependence of UC emission intensities of green and red for the NYW:Yb,Er UCNPs on Yb^{3+} (b) and (d) Er^{3+} concentrations.

The UC emission peak position does not change, whereas the emission intensity is sensitive to the variation of Yb^{3+} and Er^{3+} concentrations of the NYW:Yb,Er UCNPs. As summarized in Fig. 2b and d, when $Yb^{3+} < 20$ mol% and $Er^{3+} < 0.5$ mol%, the increase of Yb^{3+} and Er^{3+} concentration results in the increase of UC emission intensity for the NYW:Yb,Er UCNPs. The optimal doping concentrations of Yb^{3+} and Er^{3+} were determined to be 20 and 0.5 mol% for the NYW:Yb,Er UCNPs, respectively. The higher doping concentrations of $Yb^{3+} > 20$ mol% and $Er^{3+} > 0.5$ mol% result in a decrease of UC emission intensity for NYW:Yb,Er due to concentration quenching effects, which are caused by non-radiative energy transfer and the cross relaxation between Er^{3+} and/or Yb^{3+}.[34–37]

3.3 UC mechanism

The photoluminescence decay curves of both the green (552 nm) and red (656 nm) UC emissions of the NYW:*x*Yb,0.5Er (*x* = 5, 10, 15, 20, and 25) UCNPs are illustrated in Fig. 3a and b, respectively, as a function of Yb^{3+} concentration. A rise time can be observed for all decay curves of the NYW:*x*Yb,0.5Er nanoparticles, which confirms the energy transfer UC mechanism.[9,20] As summarized in Fig. 3c, with increasing Yb^{3+} concentration, the lifetime of the green and red UC emission decreases from 37 to 18 μs and from 44 to 17 μs, respectively. The lifetime values of the green and red UC emission for NYW:*x*Yb,0.5Er are longer than the reported values for $NaGd(WO_4)_2$:Yb^{3+},Er^{3+} micro-crystals, ~10 μs, but shorter than that of La_2O_3:Yb^{3+},Er^{3+} micro-crystals, ~200 μs.[20,38]

To better understand the possible UC mechanism, the power dependent UC emission spectra were determined. Fig. 3d shows the UC emission spectra of the NYW:20Yb,0.5Er UCNPs under 980 nm laser excitation at a range of PDs. It is obvious that the UC emission intensity of the NYW:20Yb,0.5Er UCNPs increases with increasing pumping power.

UC is a nonlinear process and the variation of UC emission intensity (I_{em}) based on the excitation laser power (P_{pump}) can be described using eqn (2) in the low excitation PD regime:[39]

$$I_{em} = I_{pump}^{n} \quad (2)$$

where I_{em} is the integrated UC emission intensity, I_{pump} is the pump laser power density, and n is the number of pumping photons required to excite rare earth ions from the ground state to the emitting excited state. The value of n can be obtained by the linear fit of the double logarithmic plot of UC emission intensity *versus* excitation PD. Fig. 3e presents the corresponding double logarithmic plot and linear fitting. The value of n was determined to be 1.80 ± 0.04 for green UC emission and 1.85 ± 0.04 for red UC emission indicating two-photon processes for both the green and red UC emission in NYW:Yb,Er nanoparticles. The similarity of the n values for the red and green UC indicates a stable pure green UC emission color with varying excitation PD.

Fig. 3f illustrates the UC emission mechanism of the NYW:Yb,Er UCNPs. Upon excitation of a 980 nm laser, electrons of Yb^{3+} ions are excited from the ground state of $^2F_{7/2}$ to the excited state of $^2F_{5/2}$. The first energy transfer from Yb^{3+} to Er^{3+} populates the Er^{3+}:$^4I_{11/2}$ level *via* ET1:Yb^{3+}:$^2F_{7/2}$ + Er^{3+}:$^4I_{15/2}$ →. Yb^{3+}:$^2F_{5/2}$ + Er^{3+}:$^2I_{9/2}$. The subsequent second energy transfer from Yb^{3+} to Er^{3+} populates the Er^{3+}:$^4F_{7/2}$ level *via* ET2:Yb^{3+}:$^2F_{7/2}$ + Er^{3+}:$^4I_{9/2}$ → Yb^{3+}:$^2F_{5/2}$ + Er^{3+}:$^2H_{11/2}$, which give rise to the green UC emission.

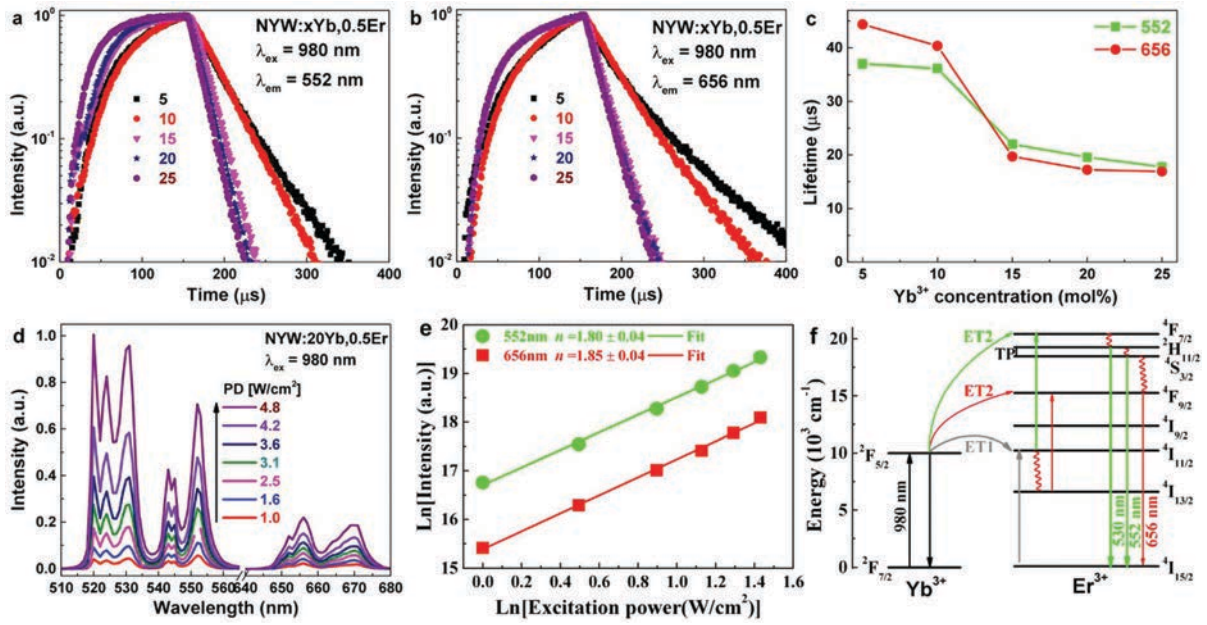

Fig. 3 Decay curves of (a) green@552 nm and (b) red@656 nm UC emission of NYW:*x*Yb,0.5Er (*x* = 5, 10, 12.5, 15, 17.5, 20, 22.5, and 25) UCNPs dependent on Yb^{3+} concentration upon 980 nm laser excitation (4 W cm ^{2}). (c) The dependence of the lifetime of red and green UC emission on Yb^{3+} concentration for the NYW:*x*Yb,0.5Er (*x* = 5, 10, 12.5, 15, 17.5, 20, 22.5, and 25) UCNPs. (d) Excitation power density (980 nm, 1 6 W cm ^{2}) dependent UC emission spectra of the NYW:20Yb,0.5Er UCNPs. (e) Double logarithmic plot of UC emission intensity in green and red *versus* excitation PD. The solid line is the linear fit of the double logarithmic plot, yielding a value for the slope n. (f) UC mechanism of the NYW:Yb,Er UCNPs upon excitation of a 980 nm laser.

There are two routes to populate the red UC emission: (i) non-radiative relaxation from the $^4I_{11/2}$ level to the $^4I_{13/2}$ level followed by energy transfer from Yb^{3+} to Er^{3+} *via* ET3:Yb^{3+}:$^2F_{7/2}$ + Er^{3+}:$^4I_{13/2}$ →. Yb^{3+}:$^2F_{5/2}$ + Er^{3+}:$^2F_{9/2}$, and (ii) non-radiative relaxation from the $^2S_{3/2}$ level to the $^4F_{7/2}$ level can populate the Er^{3+}:$^4F_{7/2}$ level leading to red UC emission.[20]

3.4 Temperature sensing behaviour

Fig. 4a shows the normalized UC emission spectra of NWY:20Yb, 0.5Er (normalized to peak at 656 nm) dependent on temperature upon excitation of a 4 W cm^{-2} 980 nm laser. With respect to G_2, the UC emission intensity of G_1 gradually increases with increasing temperature from 293 to 503 K. Consequently, the FIR of I_1/I_2 strongly increases with rising temperature from 1.4 (at 293 K) to 3.2 (at 503 K), as shown in Fig. 4b. The monotonic change in the behavior of I_{G_1}/I_{G_2} with temperature makes it highly suitable for optical thermometry, which will be discussed in detail below.

The relative electron population in the TCLs follows a Boltzmann distribution and the FIR of the two emissions from the TCLs can be well-described by eqn (3)[40]

$$\mathrm{FIR} = A + B\exp\left(\frac{\Delta E}{k_B T}\right) \quad (3)$$

where ΔE is the energy gap between TCLs, K is the Boltzmann constant, T is the absolute temperature, and A and B are constants. In the present case, the upper and lower energy levels are $^2H_{11/2}$ and $^4S_{3/2}$, respectively. The ΔE value can be obtained by fitting experimental FIR data *via* eqn (3). The experimental FIR data can be best fitted by FIR = 0.91 + 19.98 exp(1127/T). As a consequence, the ΔE value is evaluated to be about 660 cm^{-1}, which is close to the 700–800 cm^{-1} splitting between $^2H_{11/2}$ and $^4S_{3/2}$ multiplets.

The absolute temperature sensitivity S_{abs} can be calculated by eqn (4):[41]

$$S_{abs} = \frac{\partial \mathrm{FIR}}{\partial T} = (\mathrm{FIR} \quad A) \times \frac{\Delta E}{k_B T^2} \quad (4)$$

The relative sensitivity S_{rel} can be calculated *via* eqn (5):[41]

$$S_{rel} = \frac{S_A}{\mathrm{FIR}} = \frac{\Delta E}{k_B T^2} \quad (5)$$

Fig. 4c and d shows the variation of S_{abs} and S_{rel} as a function of absolute temperature, respectively. S_{abs} at 293 K was determined to be ~0.6% K^{-1}. It increases slightly with temperature from ~0.6% K^{-1} (293 K) to a maximum at ~0.9% K^{-1} (503 K). S_{rel} was determined to be 1127/T^2. S_{rel} at 293 K was determined to

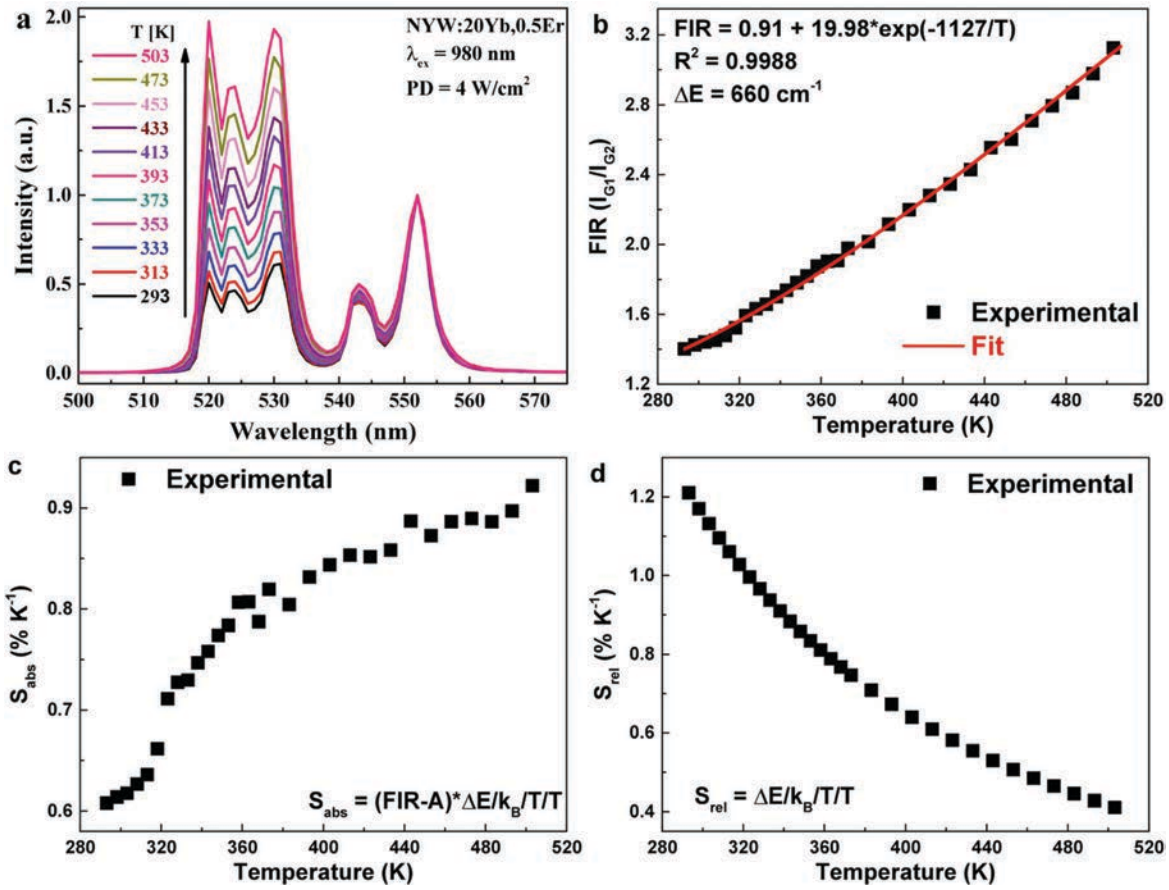

Fig. 4 (a) Temperature dependent (293 503 K) UC emission spectra of NYW:20Yb,0.5Er UCNPs upon excitation of a 980 nm laser with a PD of 4 W cm ^{2}. The spectra are normalized to the emission peak at 552 nm. (b) (d) The dependence of fluorescence intensity ratio (FIR) of G_1 to G_2 (I_{G_1}/I_{G_2}), absolute sensitivity (S_{abs}) and relative sensitivity (S_{rel}) on temperature.

Table 1 Optical thermometer parameters in some typical Er^{3+}/Yb^{3+} co doped UC materials. NPs and MPs represent nano particles and micro particles, respectively. ΔT_{min} values were recalculated *via* eqn (6) based on the reported sensitivity values in the literature

Samples	Temperature range (K)	Maximum S_{abs} (K^{-1})	S_{rel} (K^{-1})	ΔT_{min} (K)	Ref.
$NaY(WO_4)_2$:Yb^{3+}/Er^{3+} NP	293 503	0.9% K^{-1}@503 K	$1127/T^2$	0.4 K@293 K	This work
β $NaYF_4$:Yb^{3+}/Er^{3+} NP	303 483		$984/T^2$	0.5 K@293 K	43
La_2O_3:Yb^{3+}/Er^{3+} NP	313 573	0.66% K^{-1}@573 K	$1183/T^2$	0.4 K@293 K	44
Gd_2O_3:Yb^{3+}/Er^{3+} MP/NP	298 723	0.84% K^{-1}@570 K	$1175/T^2$	0.4 K@293 K	45
β $NaYF_4$:Yb^{3+}/Er^{3+} MP	293 753	0.39% K^{-1}@500 K	$1113/T^2$	0.4 K@293 K	46
$NaY(MoO_4)_2$:Yb^{3+}/Er^{3+} MP	303 523	0.97%K^{-1}@493 K	$983/T^2$	0.5 K@293 K	47
$SrWO_4$:Yb^{3+}/Er^{3+} MP	300 420	1.50% K^{-1}@403 K	$866/T^2$	0.5 K@293 K	48

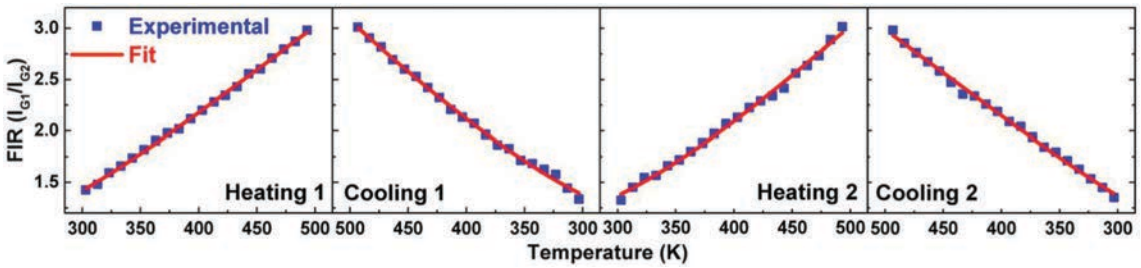

Fig. 5 The repeatability of the FIR I_1/I_2 in the temperature range of 293 503 K over two heating and cooling cycles.

be ~1.2% K^{-1} and decreases with increasing temperature from ~1.2% K^{-1} (293 K) to ~ 0.4% K^{-1} (503 K). These values are close to the reported values in the literature for other Yb^{3+}/Er^{3+}-based thermometers and nanothermometers, as summarized in Table 1. The maximum S_{abs} value of the newly developed NYW:Yb,Er (0.9% K^{-1} at 503 K) UCNPs is smaller than that of $SrWO_4$:Yb^{3+},Er^{3+} micro-crystals (1.5% K^{-1} at 403 K) but bigger than others in Table 1. The maximum S_{rel} value of the newly developed NYW:Yb,Er ($1122/T^2$ K^{-1}) UCNPs is similar to that of the reported La_2O_3:Yb^{3+},Er^{3+} nano-crystals ($1175/T^2$ K^{-1}), Gd_2O_3:Yb^{3+},Er^{3+} nano/micro-crystals ($1175/T^2$ K^{-1}) and β-$NaYF_4$:Yb^{3+},Er^{3+} micro-crystals ($1113/T^2$ K^{-1}), but bigger than others in Table 1. It is smaller than that of the typical Yb^{3+}/Tm^{3+} based nanothermometers based on TCLs of $^3F_{2,3}/^3H_4$, such as $LaPO_4$:Yb^{3+},Er^{3+} nano-crystals ($3050/T^2$ K^{-1}).[42] The repeatability of FIR is important for real applications of the thermometers. As shown in Fig. 5, excellent repeatability of the FIR of I_{G_1}/I_{G_2} can be observed over two heating and cooling cycles with a step of 20 K.

The temperature uncertainty can be determined *via* eqn (6):[41]

$$\Delta T_{min} = \frac{0.5\%}{S_{rel}} \quad (6)$$

A low temperature uncertainty of ~0.4 K at 293 K, which lies in the physiological temperature region, can be obtained.

4. Conclusions

In summary, we report a novel optical nanothermometer based on ultra-small $NaY(WO_4)_2$:Yb^{3+},Er^{3+} (NYW:Yb,Er) UCNPs obtained by a facile one-step thermolysis protocol. The XRD and TEM results indicate the successful synthesis of high purity and monodisperse diamond shaped sub-20 nm NYW:Yb,Er UCNPs with the average size of ~8.5 × 12.5 nm. NYW:Yb,Er UCNPs yield pure green UC emission under 980 nm laser excitation and the optimal composition was confirmed to be NYW:20Yb,0.5Er. The maximum relative sensitivity and absolute sensitivity were determined to be S_{rel} ~ 1.2% K^{-1} at 293 K and S_{abs} ~ 0.9% K^{-1} at 503 K, respectively. Hence, the high temperature resolution of 0.4 K at 293 K and excellent repeatability of the FIR suggest that the NYW:Yb,Er UCNPs have potential application in nanothermometry.

Conflicts of interest

There are no conflicts to declare.

Acknowledgements

This work was supported by the National Natural Science Foundation of China (No. 21771196), the Science & Technology Project of Guangdong Province (No. 2015A050502019), the Key R&D Projects of Jiangxi Province (No. 20165ABC28010), and the China Scholarship Council (No. 201506380101).

References

1 H. Dong, S. Du, X. Zheng, G. Lyu, L. Sun, L. Li, P. Zhang, C. Zhang and C. Yan, *Chem. Rev.*, 2015, **115**(19), 10725–10815.
2 S. Gai, C. Li, P. Yang and J. Lin, *Chem. Rev.*, 2014, **114**, 2343–2389.
3 Y. Liu, S. Zhou, Z. Zhuo, R. Li, Z. Chen, M. Hong and X. Chen, *Chem. Sci.*, 2016, **7**, 5013–5019.
4 Q. Liu, Y. Sun, T. Yang, W. Feng, C. Li and F. Li, *J. Am. Chem. Soc.*, 2011, **133**, 17122–17125.

5 J. Shen, L. Zhao and G. Han, *Adv. Drug Delivery Rev.*, 2013, **65**, 744–755.
6 E. A. Sykes, Q. Dai, C. D. Sarsons, J. Chen, J. V. Rocheleau, D. M. Hwang, G. Zheng, D. T. Cramb, K. D. Rinker and W. C. W. Chan, *Proc. Natl. Acad. Sci. U. S. A.*, 2016, **113**(9), E1142.
7 C. Concepción, L. P. Carlos, B. Eulalia and Z. Carlos, *Nanotechnology*, 2017, **28**, 185101.
8 G. Gao, D. Busko, S. Kauffmann-Weiss, A. Turshatov, I. A. Howard and B. S. Richards, *J. Mater. Chem. C*, 2018, **6**, 4163–4170.
9 G. Gao, A. Turshatov, I. A. Howard, D. Busko, R. Joseph, D. Hudry and B. S. Richards, *Adv. Sustainable Syst.*, 2017, **1**, 1600033.
10 T. Li, C. Guo, H. Suo and P. Zhao, *J. Mater. Chem. C*, 2016, **4**, 1964–1971.
11 X. Zhu, J. Li, X. Qiu, Y. Liu, W. Feng and F. Li, *Nat. Commun.*, 2018, **9**, 2176.
12 Y. Zuo, Z. Gou, Y. Zhang, T. Yang and W. Lin, *Chem. – Asian J.*, 2019, **14**, 67–75.
13 X. Zhu, W. Feng, J. Chang, Y. Tan, J. Li, M. Chen, Y. Sun and F. Li, *Nat. Commun.*, 2016, **7**, 10437.
14 X. Wang, X. Kong, Y. Yu, Y. Sun and H. Zhang, *J. Phys. Chem. C*, 2007, **111**, 15119–15124.
15 K. Zheng, G. He, W. Song, X. Bi and W. Qin, *J. Mater. Chem. C*, 2015, **3**, 11589–11594.
16 A. Sedlmeier, D. E. Achatz, L. H. Fischer, H. H. Gorris and O. S. Wolfbeis, *Nanoscale*, 2012, **4**, 7090–7096.
17 P. Du, L. Luo and J. S. Yu, *Ceram. Int.*, 2016, **42**, 5635–5641.
18 Y. Yang, C. Mi, F. Yu, X. Su, C. Guo, G. Li, J. Zhang, L. Liu, Y. Liu and X. Li, *Ceram. Int.*, 2014, **40**, 9875–9880.
19 T. Li, C. Guo, S. Zhou, C. Duan and M. Yin, *J. Am. Ceram. Soc.*, 2015, **98**, 2812–2816.
20 G. Gao, D. Busko, S. Kauffmann-Weiss, A. Turshatov, I. A. Howard and B. S. Richards, *J. Mater. Chem. C*, 2017, **5**, 11010–11017.
21 J. Wu, B. Cao, F. Lin, B. Chen, J. Sun and B. Dong, *Ceram. Int.*, 2016, **42**, 18666–18673.
22 N. C. George, K. A. Denault and R. Seshadri, *Annu. Rev. Mater. Res.*, 2013, **43**, 481–501.
23 Y. Tian, Y. Tian, P. Huang, L. Wang, Q. Shi and C. e. Cui, *Chem. Eng. J.*, 2016, **297**, 26–34.
24 Z. Zhang, H. Suo, X. Zhao, D. Sun, L. Fan and C. Guo, *ACS Appl. Mater. Interfaces*, 2018, **10**, 14570–14576.
25 H. Shi, L. Li, L. Zhang, T. Wang, C. Wang and Z. Su, *Dyes Pigm.*, 2015, **123**, 8–15.
26 P. Du, L. Luo, Q. Yue and W. Li, *Mater. Lett.*, 2015, **143**, 209–211.
27 G. Chen, Y. Liu, Y. Zhang, G. Somesfalean, Z. Zhang, Q. Sun and F. Wang, *Appl. Phys. Lett.*, 2007, **91**, 133103.
28 H. Zheng, B. Chen, H. Yu, J. Zhang, J. Sun, X. Li, M. Sun, B. Tian, H. Zhong, S. Fu, R. Hua and H. Xia, *RSC Adv.*, 2014, **4**, 47556–47563.
29 Z. Wang, Y. Zhang, J. Zhong, H. Yao, J. Wang, M. Wu and A. Meijerink, *Nanoscale*, 2016, **8**, 15486–15489.
30 Q. Chen, X. Xie, B. Huang, L. Liang, S. Han, Z. Yi, Y. Wang, Y. Li, D. Fan, L. Huang and X. Liu, *Angew. Chem.*, 2017, **129**, 7713–7717.
31 X. Han, A. García-Cortés, M. D. Serrano, C. Zaldo and C. Cascales, *Chem. Mater.*, 2007, **19**, 3002–3010.
32 R. Shannon, *Acta Crystallogr., Sect. A: Cryst. Phys., Diffr., Theor. Gen. Crystallogr.*, 1976, **32**, 751–767.
33 A. L. Patterson, *Phys. Rev.*, 1939, **56**, 978–982.
34 G. Gao, A. Winterstein-Beckmann, O. Surzhenko, C. Dubs, J. Dellith, M. A. Schmidt and L. Wondraczek, *Sci. Rep.*, 2015, **5**, 8942.
35 G. Gao, J. Wei, Y. Shen, M. Peng and L. Wondraczek, *J. Mater. Chem. C*, 2014, **2**, 8678–8682.
36 G. Gao and L. Wondraczek, *Opt. Mater. Express*, 2014, **4**, 476–485.
37 G. Gao, D. Busko, R. Joseph, I. A. Howard, A. Turshatov and B. S. Richards, *ACS Appl. Mater. Interfaces*, 2018, **10**, 39851–39859.
38 J. Liao, L. Nie, Q. Wang, S. Liu, H.-R. Wen and J. Wu, *RSC Adv.*, 2016, **6**, 35152–35159.
39 H. Dong, L.-D. Sun and C.-H. Yan, *Chem. Soc. Rev.*, 2015, **44**, 1608–1634.
40 B. Dong, B. Cao, Y. He, Z. Liu, Z. Li and Z. Feng, *Adv. Mater.*, 2012, **24**, 1987–1993.
41 C. D. S. Brites, A. Millán and L. D. Carlos, in *Handbook on the Physics and Chemistry of Rare Earths*, ed. B. Jean-Claude and P. Vitalij K, Elsevier, 2016, pp. 339–427.
42 M. Runowski, A. Shyichuk, A. Tymiński, T. Grzyb, V. Lavín and S. Lis, *ACS Appl. Mater. Interfaces*, 2018, **10**, 17269–17279.
43 L. Li, F. Qin, Y. Zhou, Y. Zheng, H. Zhao and Z. Zhang, *ACS Appl. Nano Mater.*, 2018, **1**, 1912–1920.
44 Z. Sun, G. Liu, Z. Fu, T. Sheng, Y. Wei and Z. Wu, *Mater. Res. Bull.*, 2017, **92**, 39–45.
45 Y. Tian, B. Tian, C. e. Cui, P. Huang, L. Wang and B. Chen, *RSC Adv.*, 2015, **5**, 14123–14128.
46 S. Fan, G. Gao, S. Sun, S. Fan, H. Sun and L. Hu, *J. Mater. Chem. C*, 2018, **6**, 5453–5461.
47 X. Yang, Z. Fu, Y. Yang, C. Zhang, Z. Wu and T. Sheng, *J. Am. Ceram. Soc.*, 2015, **98**, 2595–2600.
48 A. Pandey, V. K. Rai, V. Kumar, V. Kumar and H. C. Swart, *Sens. Actuators, B*, 2015, **209**, 352–358.

--- Supplementary Information ---

Facile synthesis of mono-disperse sub-20 nm $NaY(WO_4)_2:Er^{3+},Yb^{3+}$ upconversion nanoparticles: a new choice for nanothermometry

Mei Lin [a], Liujing Xie [a], Zijun Wang [a,b], Bryce S. Richards [c,d], Guojun Gao*[,c] and Jiuping Zhong*[,a]

[a] *School of Chemistry, School of Materials, Sun Yat-sen University, Guangzhou 510275, China*

[b] *Condensed Matter and Interfaces, Debye Institute for Nanomaterials Science, Utrecht University, Princetonplein 1, 3584 CC Utrecht, Netherlands*

[c] *Institute of Microstructure Technology, Karlsruhe Institute of Technology, 76344 Eggenstein-Leopoldshafen, Germany*

[d] *Light Technology Institute, Karlsruhe Institute of Technology, Engesserstrasse 13, 76131 Karlsruhe, Germany*

* Correspondence authors: zhongjp@mail.sysu.edu.cn (J. ZHONG);
guojun.gao@kit.edu (G. Gao)

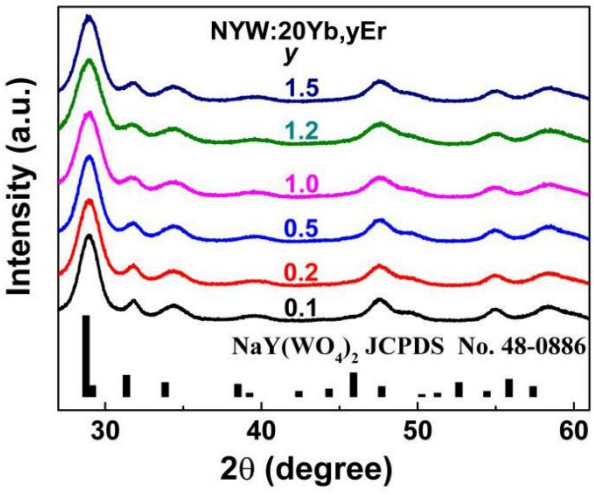

Fig. S1 XRD patterns of NYW:20Yb,*y*Er (y = 0.1, 0.2, 0.5, 1, 1.2 and 1.5) UCNPs as a function of Er^{3+} concentration, with the standard XRD pattern of $NaY(WO_4)_2$ JCPDS card no. 48-0886 provided as a reference.